IOP Publishing Journal of Micromechanics and Microengineering

J. Micromech. Microeng. **25** (2015) 065009 (13pp) doi:10.1088/0960-1317/25/6/065009

Design and modeling of a light powered biomimicry micropump

Tsun-kay Jackie Sze, Jin Liu and Prashanta Dutta

School of Mechanical and Materials Engineering, Washington State University, Pullman, WA 99164-2920, USA

E-mail: dutta@mail.wsu.edu

Received 7 January 2015, revised 24 March 2015
Accepted for publication 7 April 2015
Published 12 May 2015

Abstract

The design of compact micropumps to provide steady flow has been an on-going challenge in the field of microfluidics. In this work, a novel micropump concept is introduced utilizing bacteriorhodopsin and sugar transporter proteins. The micropump utilizes light energy to activate the transporter proteins, which create an osmotic pressure gradient and drive the fluid flow. The capability of the bio inspired micropump is demonstrated using a quasi 1D numerical model, where the contributions of bacteriorhodopsin and sugar transporter proteins are taken care of by appropriate flux boundary conditions in the flow channel. Proton flux created by the bacteriorhodopsin proteins is compared with experimental results to obtain the appropriate working conditions of the proteins. To identify the pumping capability, we also investigate the influences of several key parameters, such as the membrane fraction of transporter proteins, membrane proton permeability and the presence of light. Our results show that there is a wide bacteriorhodopsin membrane fraction range (from 0.2 to 10%) at which fluid flow stays nearly at its maximum value. Numerical results also indicate that lipid membranes with low proton permeability can effectively control the light source as a method to turn on/off fluid flow. This capability allows the micropump to be activated and shut off remotely without bulky support equipment. In comparison with existing micropumps, this pump generates higher pressures than mechanical pumps. It can produce peak fluid flow and shutoff head comparable to other non-mechanical pumps.

Keywords: micropump, proteins, osmosis, self-powered

(Some figures may appear in colour only in the online journal)

1. Introduction

Micropumps are used in applications such as in micro-total-analytical systems (μTASs), lab on a chip, and point of care testing. Numerous micropumps have been proposed with advantages and limitations as described in [1–4]. In principle micropumps can be divided into two categories: mechanical and non-mechanical pumps. Mechanical pumps convert the mechanical energy into flow and typically utilize oscillation of a diaphragm or rotation of a gear. For example gears, centrifugal, and spiral pumps have been applied to microsystems with integrated microscale coils [5]. However, mechanical pumps usually require moving parts and produce pulsating flow, which in certain cases may be undesirable. Non-mechanical pumping such as electroosmotic [6] and magnetohydrodynamic [7] have been used as an alternate method to overcome the limitations related to mechanical pumps. However non-mechanical pumps typically require large support systems, cause joule heating [8, 9], and require certain fluid properties. Osmotic pressure has also been utilized in micropumps to generate pressure through dissolving an agent [10]. However the major limitation of those pumps is the lack of active control over fluid flow rate without changing the temperature of the fluid significantly.

Plants use a complex process to store light energy by photosynthesis and utilize this energy to drive fluid transport. Therefore, this mechanism could be used as a model system for designing self-sustained microfluidic pumps.

One of the most important mechanisms for active fluid transport in plants is through sugar transport across the cell membranes by sugar transporter proteins [11] to drive fluid flow. Indeed the biohybrid systems have already been implemented in microfluidic devices. Al-Aribe *et al* [12] have incorporated the bacteriorhodopsin transporter proteins in hydrogel as a valve to control hydrogel expansion. Both sugar transporter proteins and ATPase have been used to generate osmotic pressure to cause material expansion for deformable smart materials [13, 14]. However, the devices therein are not designed for continuous pumping. Moreover, Lin *et al* [15] have employed kinesin (a motor protein) in a microfluidic device to move microtubules with cargo along protein tracks. Enzyme reactions have also been utilized as a method to drive fluid flow at speeds up to $5\,\mu\mathrm{m\,s^{-1}}$ by producing fluid density gradients through heat generation [16]. However, this method of moving fluid requires heat generation and does not produce net directional flow. Despite these previous works, to our knowledge, a steady-self-sustained micropump with net fluid flow utilizing transporter proteins is still not available.

In this work we present a micropump inspired by the active fluid transport in plants. The proposed pump requires no external energy input and, like plants, it utilizes solar energy and sugar molecules for fluid pumping. Through our numerical model, we show the feasibility of a micropump utilizing transporter proteins to provide self-sustained pumping. In our model, the active transport of protons/sugars is accounted for by solving the reaction rate equations, and the flow and pressure fields are solved using the continuity and momentum equations. The goal of this work is to propose a new bio inspired self-sustained micropump to provide fluid flow in micro/nanodevices. The rest of the paper is arranged as follows. First, we present the mathematical model for the transporter proteins and the governing equations for fluid/sucrose flow in the microfluidic device. This is followed by the validation of the bacteriorhodopsin transporter protein model with experimental results. Next, we investigate the key parameters affecting the pumping, such as the transporter protein fragment fraction, the lipid bilayer proton permeability, and illumination. Then, we compare the proposed pump with the existing micropumps and discuss the possible applications.

2. Model system

We consider the microfluidic pump as a cascade of channels as shown in figure 1. The pump chamber (aka microchannel) is located between two chambers, a lower chamber filled with water and an upper chamber with a sugar solution. For our simulations, we consider a symmetric device with the center defined at $x = 0$. Thus, we only simulate half of the device. The pumping channel has a height of h and a length of $2L_2$. The sugar solution chamber has a height of h_2 and a length of $2L_1$ and is treated as a sugar source. The water chamber is approximated as a water source with a length of $2L_2$.

The sugar solution chamber is separated from the microchannel by a lipid bilayer membrane with transporter proteins to actively convert the light energy into chemical potential. This lipid membrane contains both bacteriorhodopsin and sugar transporter proteins. Degradation of the proteins is of particular concern; hence, we specifically chose bacteriorhodopsin due to its resistance to degradation of its properties [17]. Nevertheless, there are numerous steps that can be taken to increase the stability of proteins such as by selecting storage temperature, pH, or neighboring proteins [18]. The role of bacteriorhodopsin transporter proteins is to actively pump protons from the microchannel into the sugar solution chamber, creating a proton gradient. This proton gradient facilitates sugar transport through sucrose transporter proteins, where both protons and sugars are transported from the sucrose solution chamber into the microchannel. Then the protons are pumped back into the sugar solution chamber by the bacteriorhodopsin transporter proteins. This recycling of protons allows the continual pumping of sugar molecules into the microchannel. The pumping of sugar molecules into the microchannel will increase sugar concentration in the microchannel, generating an osmotic pressure gradient between the microchannel and water chamber. A semi-permeable membrane which only allows water to pass (from water chamber to microchannel) separates the lower side of the microchannel from the water chamber. The osmotic pressure gradient will drive water from the water chamber into the microchannel and result in fluid flow along the microchannel.

3. Mathematical model

3.1. Proton pump (bacteriorhodopsin transporter protein)

As mentioned earlier, the bacteriorhodopsin transporter proteins are used in our design as the proton pump. Due to its simplicity as a compact nanoscale photo excitable proton pump, the reactions of bacteriorhodopsin have been widely studied [19, 20] and implemented in engineering devices [21, 22]. We model the proton transport in bacteriorhodopsin transporter protein based on the sequence of reactions proposed by Neutze *et al* [23]. The key components of the bacteriorhodopsin protein involved in proton transport are shown in figure 2(a). As shown, a retinal molecule is held tightly by the protein. The retinal molecule functions like a spring that stores light energy, which will be released later in the photocycle. This retinal molecule is attached to a lysine group through a Schiff base. The Schiff base along with amino acid groups aspartic acid (Asp) 96, aspartic acid 85, and arginine (Arg) 82 forms a pathway for the protons to transfer from the internal to external side of the transporter protein. The protons are then released to the external side though a proton release group formed by glutamic acid (Glu) 194 and 204.

The proton transport process in bacteriorhodopsin transporter protein is modeled with a seven-state model as shown in figure 2(b). There are a total of 13 steps involved in the process. The base protein state is denoted as *bR*, where the retinal molecule is initially in the all-trans configuration. Upon exposure to light, the photons will excite the retinal

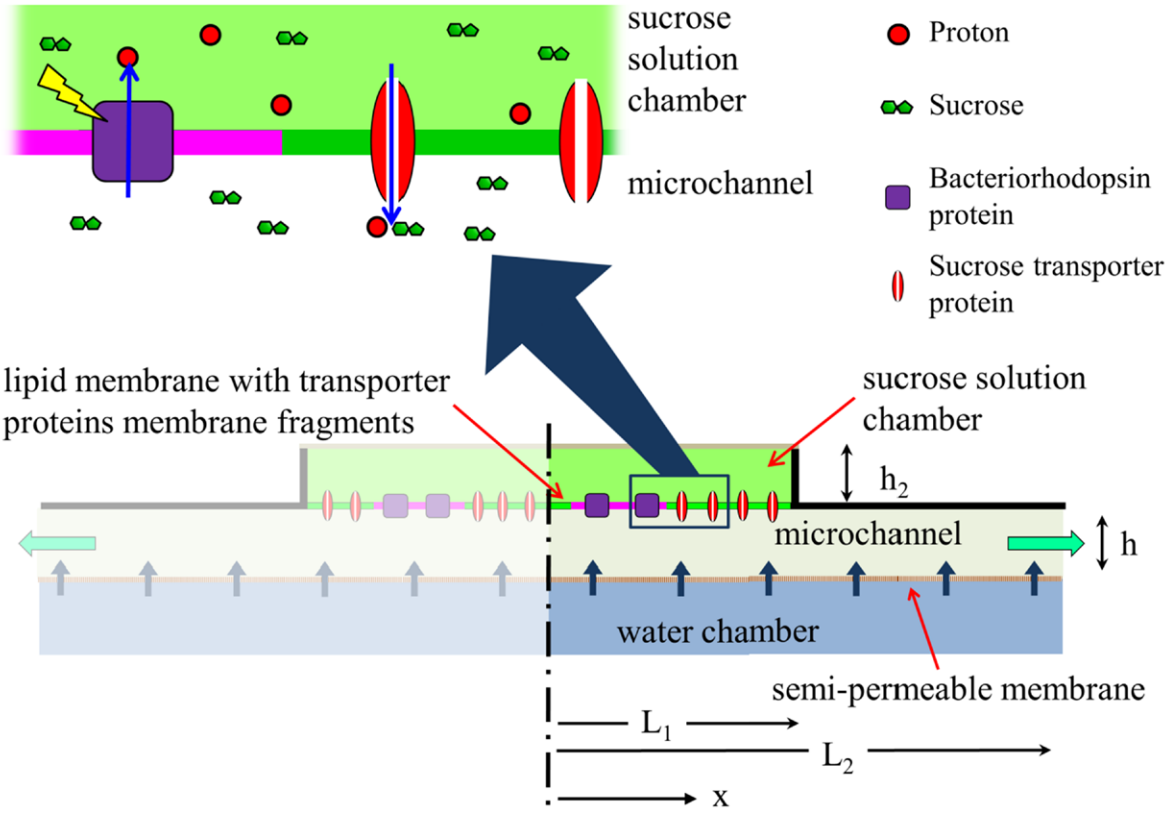

Figure 1. Schematic of the transporter protein driven active micropump. The pumping channel (microchannel) is located between two chambers. The upper sugar solution chamber is separated from the microchannel by a lipid membrane with bacteriorhodopsin and sugar transporter proteins. The lower water chamber is separated from the microchannel by a semi-permeable membrane. Both upper and lower membranes can be supported by a porous ceramic plate to withstand pressure differentials, similar to lead glass silicate plates used by others for supporting artificial membranes [13, 14]. The bacteriorhodopsin transporter proteins use light energy to pump protons from the microchannel into the sugar solution chamber creating a proton gradient. This proton gradient is used by the sugar transporter proteins to transport sugar molecules from the sucrose solution chamber into the microchannel. This will increase the sugar concentration in the microchannel. The sugar concentration difference (osmotic pressure) is used to drive water flow from the water chamber into the microchannel, resulting in net outflow. Due to the geometric symmetry, we only model the right half of the microchannel in our simulations.

molecule and change the retinal molecular shape from all-trans to 13-cis. This step represents the transition from state *bR* to state *K*. The change in molecular structure will then lead to the opening of the external side of the protein. Meanwhile the amino acids such as Arg 82 are reoriented towards the external side, leading to state *L*. This is followed by a series of thermally driven reactions moving protons in the outwards direction. State M_1 is formed when a proton located on the Schiff base is transferred to aspartic acid 85. This allows the release of a proton from the proton release group Glu 194 and 204. At the same time conformational changes occur on both sides of the protein, which closes the external side and opens the protein to the internal fluid (state M_2). A proton is then transferred from Asp 96 to the Schiff base and results in state *N*. Next, Asp 96 picks up a proton from the internal side. The retinal molecule returns to the all-trans configuration and the protein closes to the internal side, leading to state *O*. Finally the structural rearrangement of the protein opens the pathway to allow for the transport of a proton from aspartic acid 85 to the proton release group through Arg 82, which causes the protein to return its base state *bR*.

The protein surface density at a particular state can be determined from the law of mass action:

$$\begin{aligned}
\frac{\mathrm{d}bR}{\mathrm{d}t} &= k_{ObR}O + k_{NbR}N - k_{bRK}bR,\\
\frac{\mathrm{d}K}{\mathrm{d}t} &= k_{bRK}bR - k_{KL}K + k_{LK}L,\\
\frac{\mathrm{d}L}{\mathrm{d}t} &= k_{KL}K - k_{LK}L - k_{LM_1}L + k_{M_1L}M_1,\\
\frac{\mathrm{d}M_1}{\mathrm{d}t} &= k_{LM_1}L - k_{M_1L}M_1 - k_{M_1M_2}M_1 + k_{M_2M_1}M_2,\\
\frac{\mathrm{d}M_2}{\mathrm{d}t} &= k_{M_1M_2}M_1 - k_{M_2M_1}M_2 - k_{M_2N}M_2 + k_{NM_2}N,\\
\frac{\mathrm{d}N}{\mathrm{d}t} &= k_{M_2N}M_2 - k_{NM_2}N - k_{NO}N + k_{ON}O - k_{NbR}N,\\
\frac{\mathrm{d}O}{\mathrm{d}t} &= k_{NO}N - k_{ON}O - k_{ObR}O,
\end{aligned} \tag{1}$$

where surface densities of protein states are denoted accordingly (e.g. density of the *bR* state is *bR*) and k_{AB} represents the reaction rate constant from state *A* to state *B*. We consider the reaction at steady state and the total number of proteins bR_o is constant

$$bR_o = bR + K + L + M_1 + M_2 + N + O. \tag{2}$$

The protein density at each state can be solved from equations (1) and (2). The matrix form of the equations is:

$$\begin{bmatrix} 1 & 1 & 1 & 1 & 1 & 1 & 1 \\ -k_{bRK} & 0 & 0 & 0 & 0 & k_{NbR} & k_{ObR} \\ k_{bRK} & -k_{KL} & k_{LK} & 0 & 0 & 0 & 0 \\ 0 & k_{KL} & -k_{LK}-k_{LM_1} & k_{M_1L} & 0 & 0 & 0 \\ 0 & 0 & k_{LM_1} & -k_{M_1L}-k_{M_1M_2} & k_{M_2M_1} & 0 & 0 \\ 0 & 0 & 0 & k_{M_1M_2} & -k_{M_2M_1}-k_{M_2N} & k_{NM_2} & 0 \\ 0 & 0 & 0 & 0 & k_{M_2N} & -k_{NM_2}-k_{NO}-k_{NbR} & k_{ON} \end{bmatrix} \begin{bmatrix} bR \\ K \\ L \\ M_1 \\ M_2 \\ N \\ O \end{bmatrix} = \begin{bmatrix} bR_o \\ 0 \\ 0 \\ 0 \\ 0 \\ 0 \\ 0 \end{bmatrix}. \quad (3)$$

The proton transport rate from internal to external side can be expressed as:

$$J_{H^+} = k_{M_1M_2}M_1 - k_{M_2M_1}M_2. \quad (4)$$

Finally after solving equation (3) for M_1 and M_2, the proton transport rate can be calculated as:

$$J_{H^+} = bR_o \frac{k_{bRK}k_{KL}k_{LM_1}k_{M_1M_2}k_{M_2N}(k_{NbR}k_{ObR} + k_{NbR}k_{ON} + k_{NO}k)}{\Phi_1(k_j)}. \quad (5)$$

Here the denominator (Φ_1) is a complex function of the rate constants as provided in the appendix A1.

3.2. Sugar pump (sugar transporter protein)

In our design, we use the sugar transporter proteins to pump sucrose molecules into the microchannel from the sugar solution chamber. The detail structure and kinetics of the sugar transporter proteins are explained in detail in our earlier work [24], and will not be repeated. Briefly the sugar transporter proteins are modeled using a six-state model [24] describing the kinetics of the protein in response to reactant concentrations. Similar to equation (1), the surface density of the proteins at specific states is calculated as:

$$\begin{aligned} \frac{dC_1}{dt} &= k_6C_6 - k_{-6}C_1 + k_{-1}C_2 - k_1C_1H_e^+, \\ \frac{dC_2}{dt} &= k_1C_1H_e^+ - k_{-1}C_2 + k_{-2}C_3 - k_2C_2S_e, \\ \frac{dC_3}{dt} &= k_2C_2S_e - k_{-2}C_3 + k_{-3}C_4 - k_3C_3, \\ \frac{dC_4}{dt} &= k_3C_3 - k_{-3}C_4 + k_{-4}C_5S - k_4C_4, \\ \frac{dC_5}{dt} &= k_4C_4 - k_{-4}C_5S + k_{-5}C_6H^+ - k_5C_5, \\ \frac{dC_6}{dt} &= k_5C_5 - k_{-5}C_6H^+ + k_{-6}C_1 - k_6C_6. \end{aligned} \quad (6)$$

Here H^+ is the proton concentration in the microchannel, S_e is the sugar concentration in the sugar solution chamber, S is the sugar concentration in the microchannel, and k's are the reaction rate constants. By solving the equation (6) with the assumption of steady state, the rate of sugar transport by the sugar transporter protein is:

$$J_S = C_o \frac{H_e^+S_ek_1k_2k_3k_4k_5k_6 - H^+Sk_{-1}k_{-2}k_{-3}k_{-4}k_{-5}k_{-6}}{\Phi_2(k_m, k_{-m}, H_e^+, H^+, S_e, S)}, \quad (7)$$

where C_o is the total surface density of sugar transporter proteins. Φ_2 is a function of rates and reactant concentrations as listed in appendix A2.

3.3. Transport equations

Our proposed micropump is 3D with disparate length scales. For example, the length of the microchannel is in centimeter scale, the height of the microchannel is in micron scale, and the dimension of transporter proteins are on the scale of nanometers. To incorporate the various scales and to obtain computational results in reasonable time, we use quasi-1D equations developed earlier [25]. For fluid flow through the microchannel (pump chamber), as shown in figure 1, the quasi-1D continuity and momentum equations can be given as [25]:

$$\frac{\partial}{\partial t}\rho h + \frac{\partial}{\partial x}(\rho\bar{u})h - \rho_w v_w - \varpi J_S = 0, \quad (8)$$

$$\frac{\partial}{\partial t}(\rho\,\bar{u}) = -\frac{\partial p}{\partial x} - 12\frac{\mu\,\bar{u}}{h^2} - 1.2\frac{\partial}{\partial x}(\rho\,\bar{u}^2), \quad (9)$$

where v_w is the velocity of water at the wall entering into the microchannel (aka wall flow velocity), and ϖJ_S is the sugar mass influx. Fluid properties and wall flow velocity are both dependent on the sugar concentration. Thus, one has to find the sugar concentration in the microchannel. In this study, we model the sucrose and proton concentrations using the mass conservation equation:

$$\frac{\partial}{\partial t}S_ih + \frac{\partial}{\partial x}\left[\bar{u}S_i - D_i\left(\frac{\partial S_i}{\partial x} - \frac{z\Gamma}{RT}S_i\frac{\partial\varphi}{\partial x}\right)\right]h - J_i = 0, \quad (10)$$

where S_i is the concentration of species i (sucrose/proton), D_i is the diffusion coefficient in the solution, J_i is the total influx and the fourth term is the contribution due to electromigration. The pH (proton concentration) in the microchannel is kept constant at 7 due to the direct exchange of water between the microchannel and water chamber. In addition, the sugar concentration inside the sugar solution chamber is also maintained constant in our study.

3.4. Auxiliary conditions

The transport equations provided in the aforementioned section can be solved to find the flow velocity and pressure distribution in the system under appropriate boundary conditions. For the continuity and momentum equations, we consider a symmetric boundary condition at the line of symmetry ($x = 0$)

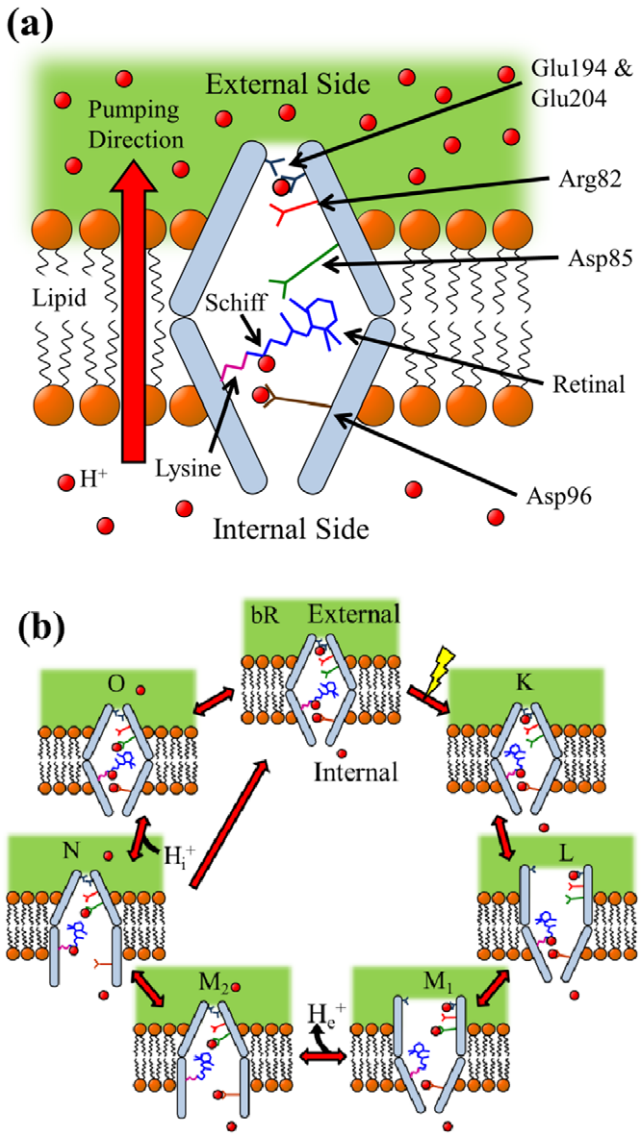

Figure 2. (a) Key components of bacteriorhodopsin transporter protein. (b) The seven-state proton transport model proposed by Neutze *et al* [23]. The base state of bacteriorhodopsin is denoted as *bR*. Due to the photon excitation, the retinal molecule experiences conformation changes. The conformational changes result in a series of proton transport steps and eventually moves a proton to the external side, where the proton leaves the transporter protein during transition from M_1 to M_2 state.

and the fully developed flow at the outlet of the microchannel with the fixed outlet thermodynamic pressure. For the mass conservation of sucrose and proton, we again assume symmetry at the center line and zero concentration gradient at the outlet.

In addition to the active transport by transporter proteins, the protons can also diffuse across lipid bilayers, and the influx is proportional to the proton concentration difference across the membrane:

$$J_{D\,H^+} = M_{H^+}(H_e^+ - H^+), \tag{11}$$

where M_{H^+} is the lipid membrane proton permeability. On the other hand, sucrose molecules are much larger; hence, the rate at which sugars leak across the membrane should be negligible compared to the rate of active transport. As a result, we assume that no sugar molecules leak into or out of the microchannel by diffusion.

The wall flow into the microchannel is driven by the osmotic and thermodynamic pressure differences, which can be calculated using the Kedem and Katchalsky equation [26]:

$$v_w = M_p[p_w - p - \sigma\,(\Pi(S_w) - \Pi(S))]. \tag{12}$$

Here M_p is the membrane hydraulic permeability, while σ is the membrane reflection coefficient. For an ideal membrane where solute molecules are prevented from passing through, $\sigma = 1$[26]. $\Pi(S)$ is the internal (microchannel) side osmotic pressure, and $\Pi(S_w)$ is the external (water chamber) side osmotic pressure. The osmotic pressure provides work potential for pumping.

3.5. Fluid properties

The primary solute in our microchannel is sucrose; therefore, the fluid properties are calculated based on the sucrose concentration (S). According to Chenlo *et al* [27], the density and viscosity of the solution are calculated using:

$$\rho = \rho_{water}(1 + 0.867\,S)^{0.164}, \tag{13}$$

$$\mu = \mu_{water}(1 + 0.867\,S)^{0.164} \left[1 + 0.73\,S\exp\left(\frac{S^{1.1}}{8.345\,T/273.1 - 7.042}\right)\right]. \tag{14}$$

The sucrose diffusion coefficient in solution is calculated from [28, 29]:

$$D_S = 5.23\times 10^{-10}\exp(-0.7248\,S). \tag{15}$$

And the osmotic pressure inside the microchannel is calculated using [30]:

$$\Pi = RT\rho_{water}(0.998\,S + 0.089S^2), \tag{16}$$

where R is the universal gas constant and T is the absolute temperature. In all cases we assume a fluid temperature of 298 K and sucrose concentration is in the unit of molal. In addition, we set the diffusion coefficient for the proton in the sucrose solution $D_{H^+} = 9.3\times 10^{-5}\,\mathrm{cm^2\,s^{-1}}$ [31], which is independent of S.

3.6. Rate constants

The reaction rate constants for the bacteriorhodopsin protein in equation (1) are pH dependent. In our simulations, the rate constant at a specific pH is obtained by linear interpolation of the experimental data from Ludmann *et al* [20]. Although the rate constant for the transition from state *bR* to *K* is not provided, the reaction takes place within picoseconds [23] and we can neglect the influence of this fast transition by

Table 1. Bacteriorhodopsin transporter protein configurations based on proton concentration on both internal (In) and external (Ext) side.

	Reaction									
Case	$L \rightarrow M_1$	$M_1 \rightarrow L$	$M_1 \rightarrow M_2$	$M_2 \rightarrow M_1$	$M_2 \rightarrow N$	$N \rightarrow M_2$	$N \rightarrow O$	$O \rightarrow N$	$O \rightarrow bR$	$N \rightarrow bR$
1	Ext	Ext	Ext	Ext	In	In	In	Ext	Ext	In
2	Ext	Ext	Ext	Ext	In	In	In	In	Ext	In
3	Ext	Ext	Ext	Ext	In	In	In	In	In	In

setting k_{bBK} as a large value. If the light source is removed and there is no excitation of the retinal molecule, then k_{bBK} will be zero. The reaction rate constants for sugar transporter proteins in equation (7) are chosen from experimental work of Boorer *et al* [32] with modifications as described in our previous work [24].

3.7. Numerical method

Quasi-1D equations are solved numerically using the finite volume method with collocated storage. In collocated finite volume, both velocity and pressure as well as other variables such as concentration and temperature are stored within the cell center [33]. Discretized algebraic equations are obtained for each control volume using the method described in [24]. We use the semi-implicit method for pressure-linked equations (SIMPLE) algorithm to iteratively solve for velocity, pressure, and species concentration. The momentum equation is first used to solve for velocity and the continuity equation is then used to solve for pressure correction. Next, the pressure correction is used to calculate pressure and modify the velocity field. Species transport equations are then solved to obtain the concentration of sugar and proton in the pumping section. After each iteration, fluid properties and fluxes are updated based on proton/sucrose concentration. We set the grid size for each differential volume as $2\,\mu$m, as coarser grid sizes of 4 and $8\,\mu$m showed no appreciable differences.

4. Results and discussion

4.1. Validation of bacteriorhodopsin protein model

In our bacteriorhodopsin protein model, the reaction rate constants are pH dependent and the pH values are different on external and internal sides of the cell to facilitate the transport of sugars. As shown in figure 2(b), the protein opens to the external side during the K to L transition. On the other hand, the protein opens to the internal side during the M_1 to M_2 transition and closes to the internal (microchannel) side during the N to O transition. The transition from M_1 to M_2 should depend on the external (sugar solution chamber side) pH because a proton leaves the protein and enters the external fluid during this process. The forward reaction from N to O should depend on the internal (microchannel side) pH due to the fact that a proton from the internal side binds to the protein. Therefore, the steps from M_2 to N and reaction N to O should depend on internal pH. The reaction from L to M_2 should depend on external pH and the reactions K to L and L to K are nearly independent of pH. However, it is not clear whether the reactions for O to N and O to bR would depend on internal or external pH. To test this, we have considered three possible configurations as listed in table 1. In each configuration we fix the internal pH at 6.5 and vary the external pH. We calculate the proton flux for each case and compare the result with the experimental measurements from Miercke *et al* [34]. In the experiment they measured the proton flux at different external pH for bacteriorhodopsin proteins cloned on *Escherichia coli* and reconstituted in soybean vesicles. Like the experimental settings of Miercke *et al* [34], we considered 31% of the proteins facing outwards (external) and the other 69% facing inwards (internal).

Results with proton flux normalized by the maximum flux for different protein configurations are shown in figure 3. Experimental data are shown in symbols. As shown, the second configuration matches best with the experimental results. This configuration (as described in table 1) corresponds to the situation that all N related reactions depend on internal pH and all other steps depend on external pH. The proton flux in the second configuration agrees with the experimental data when the pH is lower than 8. In particular both the experimental and numerical results show the same peak flux at a pH of 7.5. However, at higher pH the results deviate from the experiments. This may be due to the fact that in principle each reaction should be partially influenced by the pH on both sides of the protein; therefore, the model is less accurate for larger proton differences.

4.2. Micropump setup

We solve mass, momentum and species conservation equations in the microchannel with dimensions as shown in figure 1. In this study, the length ($2L_2$) and height (h) of microchannel are 3 cm and $1\,\mu$m, respectively. The dimensions of the sugar solution chamber are set as a height (h_2) of $1\,\mu$m and a length ($2L_1$) of 1 cm. Here, L_1 is the length of the transporter protein membrane. Thus, an increase in L_1 will increase the sucrose influx in the pumping section, which will result in more osmotic potential for pumping. In other words, one can increase the pumping power by increasing L_1. Additionally L_2 is the length of the semi-permeable membrane; an increase in L_2 will allow more wall flow. That means more osmotic energy can be converted to flow energy by increasing L_2. Considering the size of the typical micropump, L_2 was restricted to 3 cm.

The lipid membrane separating the sugar solution chamber and microchannel is composed of two parts: the first part is related to the bacteriorhodopsin transporter proteins and the

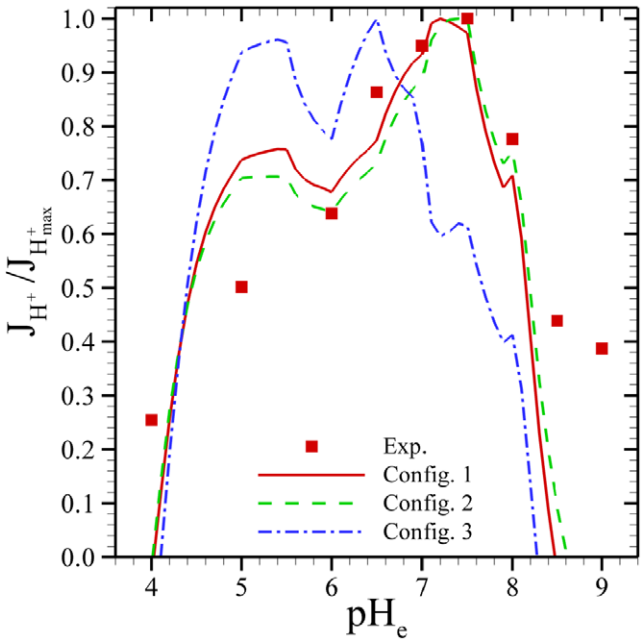

Figure 3. Comparison of normalized proton flux for different configurations with experimental data from Miercke *et al* [34] (shown as rectangles here). Miercke *et al* incorporated bacteriorhodopsin proteins in vesicles composed of soybean lipids. Vesicles were prepared against a 6.5 pH buffer. In their experimental work the external pH was varied with 31% of the bacteriorhodopsin proteins facing the outwards direction. The three configurations considered here are listed in table 1.

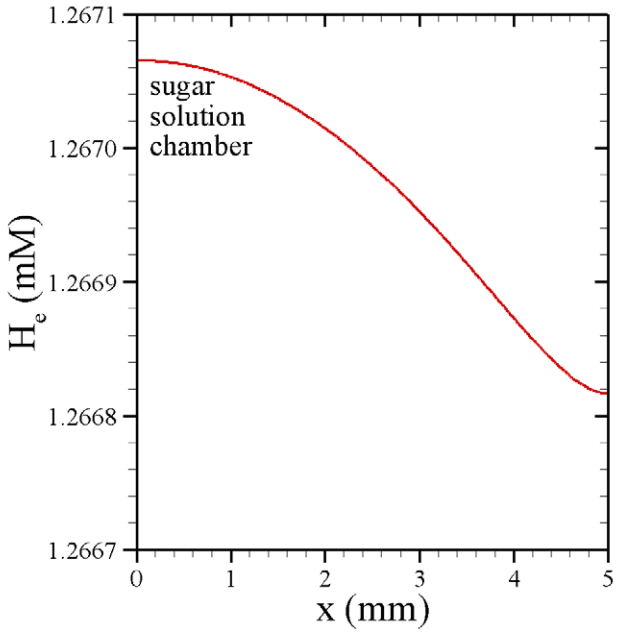

Figure 4. The variation of proton concentration inside the sugar solution chamber. Here the lipid membrane contains 0.3% bacteriorhodopsin transporter proteins fraction. The proton permeability of the lipid membrane is 7×10^{-7} cm s^{-1}, and the outlet pressure is fixed at 10 kPa.

other part is due to the sugar transporter proteins (as shown in figure 1). The protein surface density is set as 0.2 protein nm^{-2} based on *Halobacterium salinarum* [35]. For the semi-permeable membrane separating the microchannel and water chamber, the hydraulic permeability is chosen at $M_p = 10^{-12}$ m Pa^{-1} s^{-1}, which is typical for a plasma membrane with aquaporins [36]. In this study, the sugar concentration in the sugar solution chamber is fixed at 5 mM, but it can be varied to change the performance of the pump. For instance, the performance of the pump will be impacted significantly if the concentration of the sugar solution is reduced beyond a threshold value.

In principle all the transport coefficients, rate constants and membrane properties are temperature dependent. In our simulations we neglect the temperature effect as it is not possible to change the system temperature without adding or removing energy. Since the primary objective of this work is to introduce a self-sustained micropump, constant temperature operation is a valid assumption.

4.3. Flow along microchannel

Simulations are performed in a microchannel as shown in figure 1. The membrane proton permeability is set as $M_{H^+} = 7 \times 10^{-7}$ cm s^{-1}. In addition, we assume 0.3% of the lipid membrane as bacteriorhodopsin membrane fragment and the rest as sugar transporter protein fragment. The variation of the proton concentration in the sugar solution chamber is shown in figure 4 for a fixed outlet pressure of 10 kPa. During the process, the bacteriorhodopsin proteins utilize the light energy to pump the protons from the microchannel into the sugar solution chamber to generate a proton gradient. The resultant proton gradient is used by the sugar transporter proteins to drive sugar molecules from the sugar solution chamber into the microchannel. In our simulation as shown in figure 4, the proton concentration in the sugar solution chamber is higher than that in the microchannel where the proton concentration is maintained at 10^{-4} mM (pH 7). But the variation inside the sugar solution chamber is extremely small (0.25 μM) compared with the concentration difference between the microchannel and sugar solution chamber (1.3 mM).

The sugar concentration profile is shown in figure 5(a). The higher proton concentration in the sugar solution chamber allows the sugar transporter proteins to pump sucrose molecules against a sugar concentration gradient. As a result, in this case, the active pumping allows the sugar concentration to be higher in the microchannel than the sugar solution chamber. The pumping of sugars into the microchannel generates a chemical potential gradient between the microchannel and the water source, where the higher concentration of sugar in the microchannel will drive wall inflow (equation (12)). As a result water is pulled into the microchannel and pushes flow along the channel. In the region without sugar pumping, fluid inflow will dilute sugar concentration.

The velocity variation along the microchannel is shown in figure 5(b). As previously noted the higher solute concentration in the microchannel will drive fluid inflow, which will

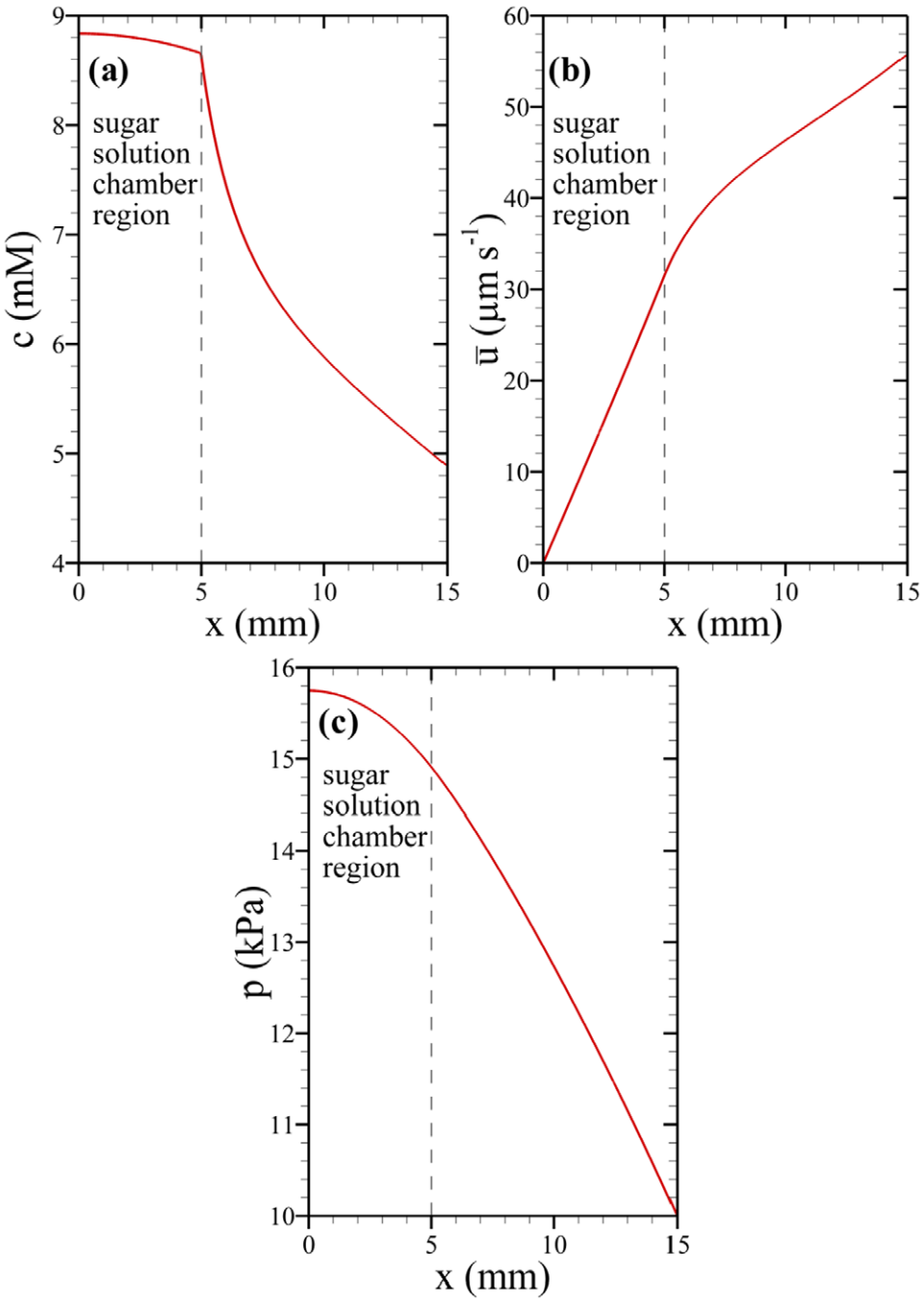

Figure 5. (a) Sugar concentration, (b) velocity, and (c) pressure distribution along the microchannel. In the region from $x = 0$ to 5 mm, the microchannel is connected with the sugar solution chamber as shown in figure 1. The other simulation parameters are the same as described in figure 4.

lead to an increase in flow velocity as fluid travels along the channel. In the section from L_1 to L_2 (without the sugar solution chamber), the flow velocity continues to increase as the sugar concentration is still sufficiently high to drive the water inflow against the thermodynamic pressure gradient. The thermodynamic pressure inside of the microchannel is shown in figure 5(c). It is important to note that the thermodynamic pressure decreases along the microchannel due to internal flow resistance. As the pressure decreases along the pump, more of the osmotic pressure can be converted into flow energy and flow rate continues to increase (figure 5(b)). In this case, the maximum osmotic pressure in the microchannel is ~22 kPa, which is used to drive fluid flow. Here the useful pressure generated by the pump is 10 kPa.

4.4. Effect of transporter protein membrane fraction

In this section, we investigate the effect of the transporter protein membrane fraction on the pumping performance. We vary the percentage of bacteriorhodopsin proteins (bR_o%), bacteriorhodopsin membrane area to total membrane area, by keeping all the other parameters the same as section 4.3. The

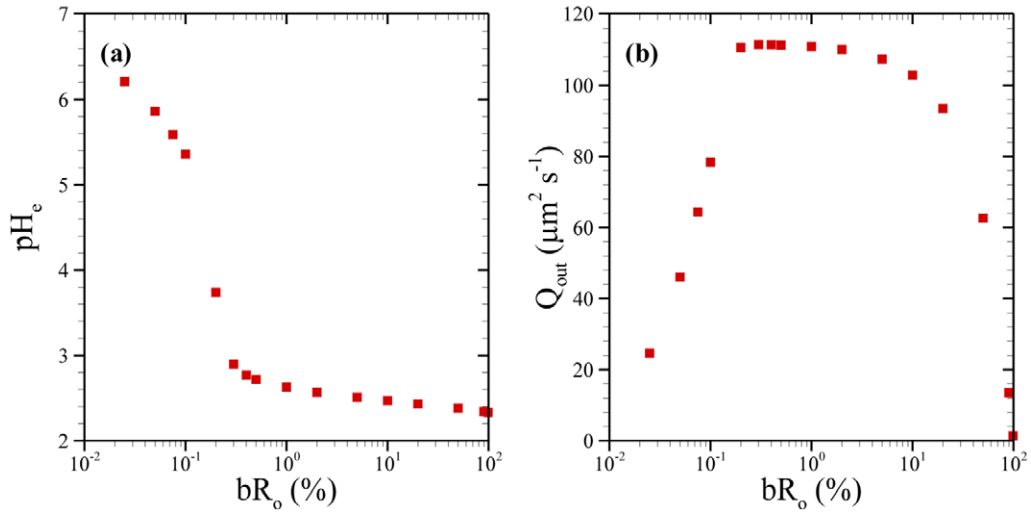

Figure 6. The effects of the bacteriorhodopsin transporter protein membrane fraction on (a) pH in the sugar solution chamber and (b) volume flow rate per unit width. The $bR_o\%$ refers to the fraction of upper membrane composed of bacteriorhodopsin membrane. All the simulation parameters are the same as described in figure 4.

pH (proton concentration) in the sugar solution chamber at different bacteriorhodopsin membrane fractions is shown in figure 6(a). As the percentage of bacteriorhodopsin proteins increases, there will be an overall increase in proton transport from the microchannel to the sugar solution chamber. Hence, the pH in the sugar solution chamber will decrease. As shown in figure 3, bacteriorhodopsin proteins operate most effectively near an external pH of 7.5, but at lower pH the proton transport is significantly hindered. Therefore as indicated in figure 6(a), at high pH, changes in the number of bacteriorhodopsin proteins will result in a more noticeable proton concentration change. However at higher bacteriorhodopsin membrane fractions, the proton pumping capability does not increase much since the bacteriorhodopsin transporter proteins are operating in a low pH condition.

Figure 6(b) shows the volume flow rate at the outlet in response to different bacteriorhodopsin membrane fractions. Flow rate is shown per unit width because flow scales proportionally with the width of the channel. In this study, we kept the height of the microchannel constant in estimating the fluid flow rate. Our numerical results show that the outflow/pumping is influenced by the balance between the number of bacteriorhodopsin proteins and sugar transporter proteins. As shown in figure 6(b), the flow reaches its maximum value when the fraction of bacteriorhodopsin protein reaches 0.2%. Decreasing the number of bacteriorhodopsin transporter proteins below 0.2% significantly reduces the pH difference across the sugar solution chamber and microchannel, and therefore results in a lower flow rate. On the other hand, when protons become highly abundant ($0.2\% < bR_o\% < 10\%$), the rate of proton–sugar transfer through the sugar transporter protein becomes dominated by steps that are independent of pH difference. Therefore, in this intermediate range, increasing the pH difference by adding more bacteriorhodopsin proteins will not increase sugar transport across individual proteins as effectively. Further increase in the bacteriorhodopsin membrane fraction above 10% significantly decreases the flow due to the reduction in sugar transporter proteins.

4.5. Effects of the membrane proton permeability and photo-activation

There is about a three orders of magnitude variation in the proton permeability from 7×10^{-7} to $10^{-3}\,\mathrm{cm\,s^{-1}}$ [37] depending on the type of membrane lipids. Therefore the type of the lipid bilayer may be important when designing a micropump. In this section we investigate the effect from the lipid type by varying the proton permeability across the membrane based on the data from Deamer [37]. Here we keep all the other parameters same as in section 4.3. We also explore the effect of the photo activation by disabling the bacteriorhodopsin transporter proteins to imitate the absence of a light source.

Figure 7(a) shows the pH (proton concentration) in the sugar solution chamber for different types of lipid membranes (different proton permeability). When the bacteriorhodopsin transporter proteins are actively pumping protons from the microchannel to the sugar solution chamber (red squares), increasing the proton permeability will enhance the proton diffusion from sugar solution chamber to microchannel and therefore decrease the proton concentration (increase the external pH). On the other hand when we completely disable the bacteriorhodopsin transporter proteins by turning off the light source (blue triangles), the protons in the sugar solution chamber will be transported together with the sugar molecules into the microchannel. This will create lower proton concentration in the sugar solution chamber making the pH in the sugar chamber slightly higher than 7 (see right vertical axis). The pH in the sugar solution chamber will decrease as the membrane permeability increases due to proton diffusion from microchannel to sugar chamber.

The change in proton concentration difference in response to the membrane proton permeability will also impact the pumping as shown in figure 7(b). When the

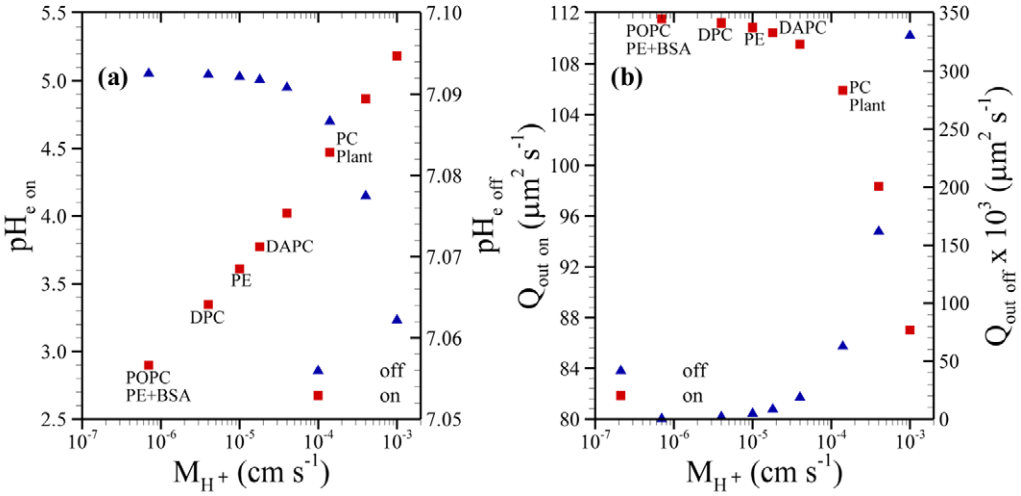

Figure 7. Effects of membrane proton permeability on (a) pH in the sugar solution chamber and (b) volume flow rate per unit width. Two distinct cases are presented for both distributions: with illumination (shown as squares) and without illumination (triangles). All other simulation conditions are the same as described in figure 4. Lipid components are abbreviated as follows: BSA—bovine serum albumin, DAPC—diarachidonoyl-phosphatidylcholine, DPC—diphytanoyl phosphatidylcholine, PC—phosphatidylcholine, PE—phosphatidylethanolamine, and POPE—1-palmitoyl-2-oleoylphosphatidylcholine.

bacteriorhodopsin transporter proteins are working (red squares), increasing the membrane proton permeability reduces the pH difference between the sugar solution chamber and microchannel. In other words, the proton concentration in the sugar solution chamber decreases resulting in low pumping of sugar which reduces the flow rate. When we turn off the light source (blue triangles) an opposing proton concentration difference will slow the sugar transport and eventually the flow will stop. However, as the membrane permeability increases, the protons will diffuse from the microchannel to sugar solution chamber. This proton diffusion will allow the sugar transporter proteins to continue pumping, albeit at a very slow rate. The results suggest that for sufficiently low membrane proton permeability one can turn on/off the pump by adding/removing the light source. Due to the lack of experimental data for rate constants, we were not able to study the effect of light intensity on the performance of our micropump. But the rate of proton pumping can be actively controlled by altering the light intensity [34], which can be used to regulate fluid flow. As a result, both flow and pressure can be controlled by adjusting the exposure to light.

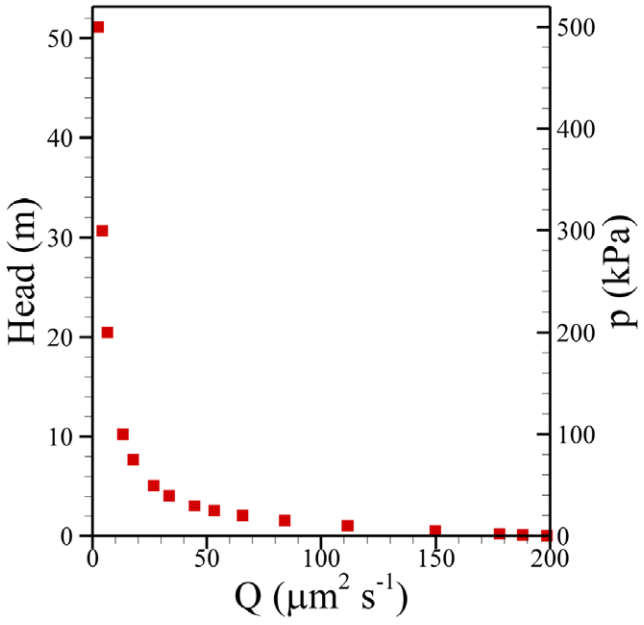

Figure 8. Pump curve for the micropump where pump head is in meters of water. The outlet pressure is varied and the volume flow rate per unit width is calculated through our simulations. The other simulation parameters are the same as described in figure 4.

4.6. Pump performance

Next, we study the pumping capability of our micropump at various flow rates. In our simulations we calculate the net discharge generated by our micropump at different outlet pressures. Figure 8 shows the pump head curve, where the pump head is calculated from the outlet pressure ($H = p/\rho g$). Like any other pump, the head generated by the pump decreases with the flow rate, but the rate of drop is much faster suggesting that this pump is suitable for low flow rate. The predicted shutoff pressure head is 500 kPa which is quite a bit lower than the pressure in the actual plant phloem (1.5 MPa) [38], suggesting that it is possible to generate high pressure head using this pump with appropriate supporting structure for membranes.

When designing a new pump, it is important to compare the performance of the pump with similarly sized existing pumps. Table 2 shows the comparison of different types of micropumps based on shutoff head and normalized flow rate. Here flow rates are normalized by pump chamber volume (as listed in table 2) which is calculated from individual pump dimensions. The characteristic length of each micropump is also listed in table 2. In comparison to mechanical pumps such as piezoelectric and peristaltic pumps, our proposed pump has

Table 2. Comparison of micropump of this work with existing pumps. Here the width of our micropump is assumed as 30 mm. The size on the last column is based on the largest dimension of the pump chamber.

Reference	Type	Shutoff head (m)	V_{pump} (mm^3)	Q_{max}/V_{pump} (min^{-1})	Size (mm)
This work	Active transport	79	0.90	0.40	30
Schabmueller *et al* [39]	Piezoelectric	0.10	2.8	550	8
Nakahara *et al* [40]	Peristaltic	—	12	130	24
Pečar *et al* [41]	Peristaltic	3.7	0.85	280	16
Al-Halhouli *et al* [42]	Synchronous motor	—	27	5.9	8.6
Zeng *et al* [43]	Electroosmotic	240	12	0.30	54

a much higher shutoff head. However for a similar sized pump, our flow rate is much lower than most mechanical pumps. As a result this pump offers advantages over mechanical pumps in that it can supply high pressure head with non-pulsating flow. One common type of non-mechanical micropump is the electroosmotic pump. In comparison to a similar sized electroosmotic pump, our pump shows comparable maximum flow rate and shutoff head. The flow rate of this pump is also similar to other membrane based pumps, such as evaporation based pumps. Nevertheless, the pump presented here is intended as a preliminary step towards an alternate method to supply fluid flow for microdevices using bio-inspired self-sustained active pumping.

4.7. Applications

The use of transporter proteins to drive fluid flow would allow for a compact micropump due to the only critical component being the transporter protein membrane. Transporter proteins have dimensions on the order of nanometers; as a result this design is compact and is only limited by the membrane surface area. The small thickness of the pump would make it ideal for lab on a chip devices, where the membrane could be patterned on the surface of the device and add negligible thickness. One application for the steady supply of sugar solution could be in cell culture devices. The capability of supplying steady flow rates would make such a device suitable for drug delivery. For example, fluid from the pump chamber could be used to displace a membrane and push a drug solution. Alternately, fluid flow could be used to dissolve water-soluble drug molecules inside a frit. Another potential application for this pump is in flow microreactors. In a microreactor, reactant molecules such as sugar or ions could be pumped into the microchannel through transporter proteins facilitated by the proton concentration.

5. Conclusions

In this paper we propose an innovative concept and initial design for a micropump using active transport mechanisms. Our bio-inspired pumps utilize concepts from phloem to generate osmotic pressure gradients and drive fluid flow. This pump requires no active power to push fluids but instead uses light energy to move sugar molecules into the pump chamber. We model the flow and solute transport in the micropump using quasi-1D equations. The proton and sugar transport facilitated by transporter proteins are modeled by solving the corresponding rate equations. We validate the model for bacteriorhodopsin transporter protein against the experimental results.

Our model indicates that there are some geometric parameters that are important when designing this micropump. For instance, increasing the size of the transporter protein membrane (L_1) will lead to higher sucrose influx, thus drive significantly higher flow rates. Lengthening the semipermeable membrane (L_2) will increase flow rate through converting more of the chemical energy (due to osmotic pressure) into flow energy. Moreover, at moderately lower sugar concentration in the sugar solution chamber, raising its value will accelerate the rate of sugar transport facilitated by transporter proteins and increase fluid flow. While a more detail parametric study is needed to optimize the design of this pump, the primary objective of this work is to demonstrate the self-sustained active pumping without any external energy.

We also investigate the effects from several key factors including transporter protein fraction in lipid membrane, types of lipid membranes, and illumination on the performance of the pump. Simulation results show that there is a wide bacteriorhodopsin membrane fraction range (from 0.2 to 10%) at which flow rate stays nearly constant. Below 0.2%, fluid flow is hindered due to the lack of active proton pumping required to generate the proton gradient, and above 10% the benefit of adding proton pumps is outweighed by the reduction in sugar transporter proteins. Our study of the membrane proton permeability and light source suggests illumination can be used as a controlling mechanism to turn on/off the micropump. By adjusting light exposure, the flow rate could be actively altered. At moderately low membrane permeability, the pump can be completely stopped by removing the light source. In comparison to existing pumps, the maximum pressure and flow rate of this pump is comparable with existing non-mechanical pumps. The predicted maximum flow rate is comparable with electroosmotic pumps; however, the flow rate is much lower than mechanical pumps. Overall, the results of this work indicate that a solar powered device utilizing transporter proteins has great potential for next generation non-mechanical micropumps.

Acknowledgments

This work was supported in part by the National Science Foundation under Grant No. CBET 1250107.

Appendix A1. Denominator for bacteriorhodopsin proton flux equation

$$\Phi = k_{bR}k_{KL}k_{LM1}k_{M1M2}k_{M2N}k_{NO} + k_{bR}k_{KL}k_{LM1}k_{M1M2}k_{M2N}k_{ObR} + k_{bR}k_{KL}k_{LM1}k_{M1M2}k_{M2N}k_{ON} + k_{bR}k_{KL}k_{LM1}k_{M1M2}k_{NbR}k_{ObR} + k_{bR}k_{KL}k_{LM1}k_{M2N}k_{NbR}k_{ObR} + k_{bR}k_{KL}k_{LM1}k_{M1M2}k_{NM2}k_{ObR} + k_{bR}k_{KL}k_{LM1}k_{M1M2}k_{NbR}k_{ON} + k_{bR}k_{KL}k_{LM1}k_{M2M1}k_{NM2}k_{ObR} + k_{bR}k_{KL}k_{LM1}k_{M2N}k_{NbR}k_{ON} + k_{bR}k_{KL}k_{LM1}k_{M2M1}k_{NbR}k_{ON} + k_{bR}k_{KL}k_{LM1}k_{M1M2}k_{NO}k_{ObR} + k_{bR}k_{KL}k_{LM1}k_{M2N}k_{NO}k_{ObR} + k_{bR}k_{KL}k_{LM1}k_{M2M1}k_{NO}k_{ObR} + k_{bR}k_{KL}k_{LM1}k_{M1M2}k_{NM2}k_{ON} + k_{bR}k_{KL}k_{LM1}k_{M2M1}k_{NM2}k_{ON} + k_{bR}k_{KL}k_{M1L}k_{M2N}k_{NbR}k_{ObR} + k_{bR}k_{KL}k_{M1L}k_{M2M1}k_{NbR}k_{ObR} + k_{bR}k_{KL}k_{M1M2}k_{M2N}k_{NbR}k_{ObR} + k_{bR}k_{KL}k_{M1L}k_{M2M1}k_{NM2}k_{ObR} + k_{bR}k_{KL}k_{M1L}k_{M2N}k_{NbR}k_{ON} + k_{bR}k_{KL}k_{M1L}k_{M2M1}k_{NbR}k_{ON} + k_{bR}k_{KL}k_{M1M2}k_{M2N}k_{NbR}k_{ON} + k_{bR}k_{KL}k_{M1L}k_{M2N}k_{NO}k_{ObR} + k_{bR}k_{KL}k_{M1L}k_{M2M1}k_{NO}k_{ObR} + k_{bR}k_{KL}k_{M1M2}k_{M2N}k_{NO}k_{ObR} + k_{bR}k_{KL}k_{M1L}k_{M2M1}k_{NM2}k_{ON} + k_{bR}k_{LK}k_{M1L}k_{M2N}k_{NbR}k_{ObR} + k_{bR}k_{LK}k_{M1L}k_{M2M1}k_{NbR}k_{ObR} + k_{bR}k_{LK}k_{M1M2}k_{M2N}k_{NbR}k_{ObR} + k_{bR}k_{LM1}k_{M1M2}k_{M2N}k_{NbR}k_{ObR} + k_{bR}k_{LK}k_{M1L}k_{M2M1}k_{NM2}k_{ObR} + k_{bR}k_{LK}k_{M1L}k_{M2N}k_{NbR}k_{ON} + k_{bR}k_{LK}k_{M1L}k_{M2M1}k_{NbR}k_{ON} + k_{bR}k_{LK}k_{M1M2}k_{M2N}k_{NbR}k_{ON} + k_{bR}k_{LK}k_{M1L}k_{M2N}k_{NO}k_{ObR} + k_{bR}k_{LK}k_{M1L}k_{M2M1}k_{NO}k_{ObR} + k_{bR}k_{LK}k_{M1M2}k_{M2N}k_{NO}k_{ObR} + k_{bR}k_{LM1}k_{M1M2}k_{M2N}k_{NbR}k_{ON} + k_{bR}k_{LM1}k_{M1M2}k_{M2N}k_{NO}k_{ObR} + k_{bR}k_{LK}k_{M1L}k_{M2M1}k_{NM2}k_{ON} + k_{KL}k_{LM1}k_{M1M2}k_{M2N}k_{NbR}k_{ObR} + k_{KL}k_{LM1}k_{M1M2}k_{M2N}k_{NbR}k_{ON} + k_{KL}k_{LM1}k_{M1M2}k_{M2N}k_{NO}k_{ObR}$$

Appendix A2. Denominator for sucrose transporter protein transport equation

$$\Phi_2 = k_{-1}k_{-2}k_{-3}k_{-6}k_5 + k_{-1}k_{-2}k_{-3}k_5k_6 + k_{-1}k_{-2}k_{-6}k_4k_5 + k_{-1}k_{-2}k_4k_5k_6 + k_{-1}k_{-6}k_3k_4k_5 + k_{-1}k_3k_4k_5k_6 + H^+k_{-1}k_{-2}k_{-3}k_{-5}k_{-6} + H^+k_{-1}k_{-2}k_{-5}k_{-6}k_4 + H_e^+k_{-2}k_{-3}k_1k_5k_6 + H^+k_{-1}k_{-5}k_{-6}k_3k_4 + H_e^+k_{-2}k_1k_4k_5k_6 + H_e^+k_1k_3k_4k_5k_6 + Sk_{-1}k_{-2}k_{-3}k_{-4}k_{-6} + Sk_{-1}k_{-2}k_{-3}k_{-4}k_6 + S_ek_{-6}k_2k_3k_4k_5 + S_ek_2k_3k_4k_5k_6 + H^+Sk_{-1}k_{-2}k_{-3}k_{-4}k_{-5} + H^+Sk_{-1}k_{-2}k_{-4}k_{-5}k_{-6} + H^+Sk_{-1}k_{-3}k_{-4}k_{-5}k_{-6} + H^+Sk_{-2}k_{-3}k_{-4}k_{-5}k_{-6} + H_e^+Sk_{-2}k_{-3}k_{-4}k_1k_6 + H^+Sk_{-1}k_{-4}k_{-5}k_{-6}k_3 + H_e^+S_ek_{-3}k_1k_2k_5k_6 + H^+S_ek_{-5}k_{-6}k_2k_3k_4 + H_e^+S_ek_1k_2k_3k_4k_5 + H_e^+S_ek_1k_2k_3k_4k_6 + H_e^+S_ek_1k_2k_3k_5k_6 + H_e^+S_ek_1k_2k_4k_5k_6 + H_e^+H^+Sk_{-2}k_{-3}k_{-4}k_{-5}k_1 + H_e^+H^+S_ek_{-5}k_1k_2k_3k_4 + H^+S_eSk_{-3}k_{-4}k_{-5}k_{-6}k_2 + H_e^+S_eSk_{-3}k_{-4}k_1k_2k_6 + H^+S_eSk_{-4}k_{-5}k_{-6}k_2k_3 + H_e^+S_eSk_{-4}k_1k_2k_3k_6 + H_e^+H^+S_eSk_{-3}k_{-4}k_{-5}k_1k_2 + H_e^+H^+S_eSk_{-4}k_{-5}k_1k_2k_3$$

References

[1] Nguyen N-T, Huang X and Chuan T K 2002 MEMS-micropumps: a review *ASME J. Fluids Eng.* **124** 384–92

[2] Laser D and Santiago J 2004 A review of micropumps *J. Micromech. Microeng.* **14** R35

[3] Nisar A, Afzulpurkar N, Mahaisavariya B and Tuantranont A 2008 MEMS-based micropumps in drug delivery and biomedical applications *Sensors Actuators* B **130** 917–42

[4] Woias P 2005 Micropumps—past, progress and future prospects *Sensors Actuators* B **105** 28–38

[5] Al-Halhouli A A, Demming S, Waldschik A and Büttgenbach S 2014 Implementation of synchronous micromotor in developing integrated microfluidic systems *Micromachines* **5** 442–56

[6] Snyder J L, Getpreecharsawas J, Fang D Z, Gaborski T R, Striemer C C, Fauchet P M, Borkholder D A and McGrath J L 2013 High-performance, low-voltage electroosmotic pumps with molecularly thin silicon nanomembranes *Proc. Natl Acad. Sci. USA* **110** 18425–30

[7] Rivero M and Cuevas S 2012 Analysis of the slip condition in magnetohydrodynamic (MHD) micropumps *Sensors Actuators* B **166** 884–92

[8] Horiuchi K and Dutta P 2004 Joule heating effects in electroosmotically driven microchannel flows *Int. J. Heat Mass Transfer* **47** 3085–95

[9] Horiuchi K, Dutta P and Hossain A 2006 Joule-heating effects in mixed electro-osmotic and pressure-driven microflows under constant wall heat flux *J. Eng. Math.* **54** 159–80

[10] Su Y C and Lin L W 2004 A water-powered micro drug delivery system *J. Microelectromech. Syst.* **13** 75–82

[11] Turgeon R 2010 The role of phloem loading reconsidered *Plant Physiol.* **152** 1817–23

[12] Al-Aribe K and Knopf G K 2010 Photoresponsive hydrogel microvalve activated by bacteriorhodopsin proton pumps *Proc. SPIE* **7646** 764611 (International Society for Optics and Photonics)

[13] Sundaresan V B and Leo D J 2007 Controlled fluid transport using ATP-powered protein pumps *Smart Mater. Struct.* **16** S207

[14] Sundaresan V B and Leo D J 2008 Modeling and characterization of a chemomechanical actuator using protein transporter *Sensors Actuators* B **131** 384–93

[15] Lin C-T, Kao M-T, Kurabayashi K and Meyhofer E 2008 Self-contained, biomolecular motor-driven protein sorting and concentrating in an ultrasensitive microfluidic chip *Nano Lett.* **8** 1041–6

[16] Sengupta S, Patra D, Ortiz-Rivera I, Agrawal A, Shklyaev S, Dey K K, Córdova-Figueroa U, Mallouk T E and Sen A 2014 Self-powered enzyme micropumps *Nat. Chem.* **6** 415–22

[17] Aranda F, Garimella R, McCarthy N, Rao D N, Rao D, Chen Z, Akkara J, Kaplan D and Roach J 1995 All-optical

light modulation in bacteriorhodopsin films *Appl. Phys. Lett.* **67** 599–601
[18] Wang Y, Sarkar M, Smith A E, Krois A S and Pielak G J 2012 Macromolecular crowding and protein stability *J. Am. Chem. Soc.* **134** 16614–8
[19] Lozier R H, Xie A, Hofrichter J and Clore G M 1992 Reversible steps in the bacteriorhodopsin photocycle *Proc. Natl Acad. Sci. USA* **89** 3610–4
[20] Ludmann K, Gergely C and Váró G 1998 Kinetic and thermodynamic study of the bacteriorhodopsin photocycle over a wide pH range *Biophys. J.* **75** 3110–9
[21] Roy S, Prasad M, Topolancik J and Vollmer F 2010 All-optical switching with bacteriorhodopsin protein coated microcavities and its application to low power computing circuits *J. Appl. Phys.* **107** 053115
[22] Chu L-K, Yen C-W and El-Sayed M A 2010 Bacteriorhodopsin-based photo-electrochemical cell *Biosens. Bioelectron.* **26** 620–6
[23] Neutze R, Pebay-Peyroula E, Edman K, Royant A, Navarro J and Landau E M 2002 Bacteriorhodopsin: a high-resolution structural view of vectorial proton transport *Biochim. Biophys. Acta* **1565** 144–67
[24] Sze T K J, Liu J and Dutta P 2014 Numerical modeling of flow through phloem considering active loading *ASME J. Fluids Eng.* **136** 021206
[25] Sze T-K J, Dutta P and Liu J 2013 Study of protein facilitated water and nutrient transport in plant phloem *ASME J. Nanotechnol. Eng. Med.* **4** 031005
[26] Kargol M and Kargol A 2003 Mechanistic equations for membrane substance transport and their identity with Kedem–Katchalsky equations *Biophys. Chem.* **103** 117–27
[27] Chenlo F, Moreira R, Pereira G and Ampudia A 2002 Viscosities of aqueous solutions of sucrose and sodium chloride of interest in osmotic dehydration processes *J. Food Eng.* **54** 347–52
[28] Ekdawi-Sever N, de Pablo J J, Feick E and von Meerwall E 2003 Diffusion of sucrose and alpha,alpha-trehalose in aqueous solutions *J. Phys. Chem.* A **107** 936–43
[29] Chatterjee A 1964 Measurement of the diffusion coefficients of sucrose in very dilute aqueous solutions using jamin interference optics at 25° *J. Am. Chem. Soc.* **86** 793–5
[30] Michel B E 1972 Solute potentials of sucrose solutions *Plant Physiol.* **50** 196–8
[31] Gutman M, Nachliel E and Kiryati S 1992 Dynamic studies of proton diffusion in mesoscopic heterogeneous matrix: II. The interbilayer space between phospholipid membranes *Biophys. J.* **63** 281–90
[32] Boorer K J, Loo D D, Frommer W B and Wright E M 1996 Transport mechanism of the cloned potato H^+/sucrose cotransporter StSUT1 *J. Biol. Chem.* **271** 25139–44
[33] Yoo K, Shim J, Liu J and Dutta P 2014 Mathematical and numerical model to study two-dimensional free flow isoelectric focusing *Biomicrofluidics* **8** 034111
[34] Miercke L J, Betlach M C, Mitra A K, Shand R F, Fong S K and Stroud R M 1991 Wild-type and mutant bacteriorhodopsins D85N, D96N, and R82Q: Purification to homogeneity, pH dependence of pumping and electron diffraction *Biochemistry* **30** 3088–98
[35] Henderson R and Unwin P N T 1975 3D model of purple membrane obtained by electron microscopy *Nature* **257** 28–32
[36] Wang H L, Chung T-S, Tong Y W, Jeyaseelan K, Armugam A, Duong H H P, Fu F, Seah H, Yang J and Hong M 2013 Mechanically robust and highly permeable AquaporinZ biomimetic membranes *J. Membr. Sci.* **434** 130–6
[37] Deamer D 1987 Proton permeation of lipid bilayers *J. Bioenerg. Biomembr.* **19** 457–79
[38] Gould N, Thorpe M R, Koroleva O and Minchin P E H 2005 Phloem hydrostatic pressure relates to solute loading rate: a direct test of the Munch hypothesis *Funct. Plant Biol.* **32** 1019–26
[39] Schabmueller C, Koch M, Mokhtari M, Evans A, Brunnschweiler A and Sehr H 2002 Self-aligning gas/liquid micropump *J. Micromech. Microeng.* **12** 420
[40] Nakahara K, Yamamoto M, Okayama Y, Yoshimura K, Fukagata K and Miki N 2013 A peristaltic micropump using traveling waves on a polymer membrane *J. Micromech. Microeng.* **23** 085024
[41] Pečar B, Križaj D, Vrtačnik D, Resnik D, Dolžan T and Možek M 2014 Piezoelectric peristaltic micropump with a single actuator *J. Micromech. Microeng.* **24** 105010
[42] Al Halhouli A, Kilani M, Waldschik A, Phataralaoha A and Büttgenbach S 2012 Development and testing of a synchronous micropump based on electroplated coils and microfabricated polymer magnets *J. Micromech. Microeng.* **22** 065027
[43] Zeng S, Chen C-H, Mikkelsen J C Jr and Santiago J G 2001 Fabrication and characterization of electroosmotic micropumps *Sensors Actuators* B **79** 107–14